Molecular-scale bio-sensing using armchair graphene

R. Chowdhury,[1,a)] F. Scarpa,[2,b)] and S. Adhikari[1,c)]
[1]*Swansea University, Singleton Park, Swansea SA2 8PP, United Kingdom*
[2]*University of Bristol, University Walk, Bristol BS8 1TR, United Kingdom*

(Received 10 February 2012; accepted 5 June 2012; published online 10 July 2012)

We evaluate the transport properties performance of armchair graphene nanoribbons (AGNRs) with a bio-molecule assembly as potential molecular-scale biosensors (Anthracene). The bio-molecules are assumed to be absorbed at the edge of an AGNR, and to behave as quasi-1D systems. The transport spectrum and density of states (DOS) are calculated using a single-band tight-binding Hamiltonian representation, and a non-equilibrium Greens function formalism. Doping with boron and nitride atoms and its impact on the transport properties has also been evaluated. Significant changes in transmission and increase in DOS by 200% are observed when the Anthracene molecule is interacting with the AGNR. Boron and Nitrogen doping allow to increase current flows at constant voltage by 50% on average. There results suggest potential significant scope on using AGNRs for bio-devices based on either conductance or electroluminescence. © *2012 American Institute of Physics*. [http://dx.doi.org/10.1063/1.4733689]

I. INTRODUCTION

Last decade saw the discovery of superlattice monolayers[1] and thin films of 2D honeycomb-lattice carbon ("graphene").[2] Graphene sheets and multilayers have very rapidly shown a significant promise for nanoelectronics and nano electro-mechanical systems (NEMS) applications, because of their singular combination between mechanical and elastic properties,[3–9] and unusual electronic structure. Graphene can be also synthetized as 1D material (nanoribbon), with evidence of large density of states (DOS) at the edge near the Fermi level for this specific nanostructure.[10] The electronic linear spectrum and the chiral characteristic of the electron's wave function are unique to graphene systems, and are responsible for the Klein tunneling effect[11,12] observed in graphene heterojunctions.[13] Conductivity is another property which assumes in graphene systems a peculiar aspect. Graphene with impurities tend to have typical distances of the doping with a similar order of magnitude of the de Broglie wavelength of electrons, making graphene highly conductive but disordered metals, with the behaviour of the electrons depending on metal contacts, surfaces, and quantum mechanical interference.[14] Moreover, different quantization rules have been identified for pure (undoped) graphene nanoribbons (GNRs) with zigzag[15] and, in particular, for armchair edges.[16,17] The influence of quantum effects external to the graphene nanoribbon is a mechanism that several authors have identified for potential breakthrough in mass sensors[18,19] design, both theoretical,[20,21] and experimental.[22]

In this article, we study the effect of organic molecule adsorption on the transport of single layer GNRs in a two-probe configuration. In particular, armchair GNR (AGNR) with quasi-one dimensional organic-fragment is considered here. We choose linear polyaromatic hydrocarbons such as Anthracene (Ref. Fig. 1). Understanding their interaction with GNRs will help to understand how full organic or bio-fragments/proteins (which are too complex to be presently simulated by the state-of-the-art *ab initio* techniques used here) interact with AGNRs. These molecules could be useful to simulate the effects on the electronic transport of AGNRs, for development of graphene based sensor devices. Some groups have made progress necessary towards experimental demonstration of graphene nanoribbon based sensors. Kosynkin *et al.*[23] obtained graphene nanoribbons by longitudinal unzipping of carbon nanotubes. Along this line, a laser-induced unzipping of carbon nanotubes to yield graphene nanoribbons was proposed by Kumar *et al.*[24] Cai *et al.*[25] proposed an atomically precise bottom-up fabrication technique for graphene nanoribbons. Synthesis of high-quality graphene nanoribbons was also proposed by Jiao *et al.*[26] and Doessel *et al.*[27] Talyzin *et al.*[28] synthesised graphene nanoribbons encapsulated in single-walled carbon nanotubes. These works make it possible to use graphene nanoribbons as nanoscale sensor by utilising its electronic properties.

In our earlier study,[20] it has been shown that zigzag edged GNR (ZGNR) has a very large density of states at the Fermi level, which is attributed to the localized edge-states having nonbonding character. These peculiar electronic properties significantly affect their transport properties. However, it is shown in the paper that AGNR (Ref. 29) has near zero density of states at the Fermi level, which can, however, be modified by impurities or chemical functionalization. It can be pointed out that, ZGNR-based system, I-V characteristics is significant even at lower bias ($V = 0 - 0.2$), whereas for AGNR-based system this is negligible. Furthermore, it can also be observed that, ZGNR-based system shows clear indication about negative differential resistance, whereas for AGNR-based system we do not find such characteristics.

II. MODELLING AND SIMULATION

Geometry relaxations and electronic structures of the AGNR and the hybrid system of AGNR with attached

[a)]R.Chowdhury@swansea.ac.uk.
[b)]F.Scarpa@bristol.ac.uk.
[c)]S.Adhikari@swansea.ac.uk.

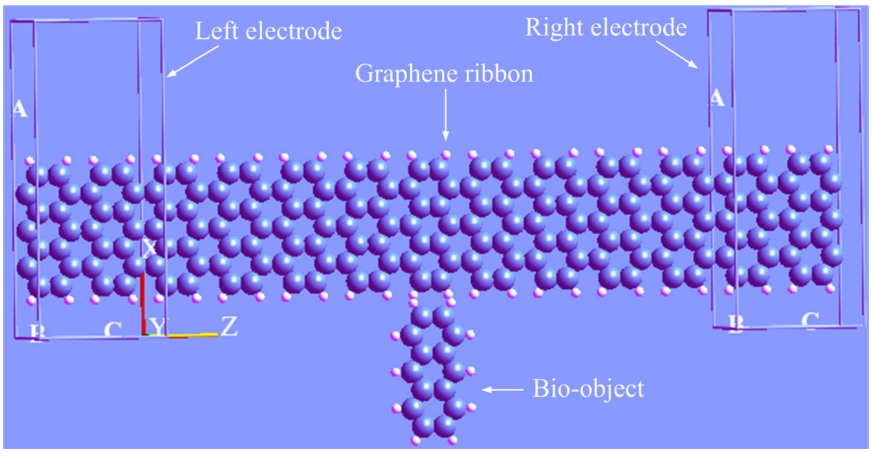

FIG. 1. Schematic configuration of a two-probe system for an armchair nanoribbon of ten unit cells in length with attached molecule. The configuration is divided into three regions: left electrode, right electrode, and central scattering region. Attached organic-fragment is Anthracene ($C_{14}H_{10}$), which is essentially an organic semiconductor. It is a solid polycyclic aromatic hydrocarbon consisting of three fused benzene rings and used as a scintillator for detectors of high energy photons, electrons, and alpha particles.

organic molecule are calculated by using density functional theory (DFT) using Atomistix ToolKit (ATK).[30] In our transport calculations, the exchange-correlation potential is described by the local density approximation (LDA).[31] Troullier Martins non-local pseudo potential[32] are used to model core electrons, and valence electrons are expanded in a SIESTA (Ref. 33) localized basis set. The C–C and C–H bond lengths are set to be 1.42 and 1.1 Å, respectively. All atomic positions are fully relaxed with a force tolerance of 0.001 eV/Å. The system is analyzed with $1 \times 1 \times 300$ uniformly spaced k-points (300 k-points in transport direction). We performed convergence study with respect to k-points sampling. For this purpose, the setup is increased by increasing the k-points in transport direction up to 500; however, there is no change in transmission spectrum. The self-consistent calculations are performed with a mixing rate set to 0.01 and the convergent criterion for total energy is 10^{-5} eV.

The use of basis set in the *ab initio* simulations has significant effect on the results, as demonstrated in Refs. 34–36. Due to this fact, first we performed bare ZNRs, where we repeated the simulations using the double-ζ, and single-ζ basis sets. It was found that the difference between the relative current changes predicted by the double-ζ and the single-ζ basis sets is not significant in the range of the bias used. In our calculations, single-ζ polarized basis set is used and the mesh cutoff is set to be 150 Ry to save computational time. Moreover, ATK uses periodic boundary conditions in the directions transverse to the transport direction. To assure that no significant interaction occurs between the actual simulation box and its repeated images, as was previously pointed out,[37] we used vacuum pad of >10 Å in the x and y directions. It is also noted that vacuum padding is needed to allow electrostatic interactions to decay for systems. The size of the simulation box is increased in the transverse direction till the relative changes in the calculated current are observed as $\sim 1\%$. The transport mechanism[38] of the system is studied using DFT based non-equilibrium Green's function (NEGF) formalism. Using NEGF theory, the transmission coefficients can obtained as

$$T(E) = \mathbf{tr}(\Upsilon_R G_C \Upsilon_L G_C^{+}). \quad (1)$$

Here the subscripts C, L, and R used to denote central scattering, left, and right electrodes, respectively. G_C and $\Upsilon_{L(R)}$ denote the corresponding Greens functions and imaginary parts of the self-energies, respectively. The current passing through the scattering central region is calculated by the Landauer formula[39]

$$I(V) = \frac{2e}{h}\int_{\mu_L}^{\mu_R} \Big(f(E-\mu_L) - f(E-\mu_R)\Big) T(E)\, dE. \quad (2)$$

Here μ_L and μ_R are the chemical potential of left and right electrodes, k_B is the Boltzmann constant, T_{temp} is the temperature, $f(E-\mu) = 1/\{1+\exp\lfloor E-\mu/k_B T_{temp}\rfloor\}$ is the Fermi Dirac distribution function, and $T(E)$ is the transmission function. Following are program parameters used in the present analyses: (i) Iteration mixing parameter: Algorithm = Pulay and diagonal mixing parameter = 0.1; (ii) basis set parameters: Type = single-ζ polarized, radial sampling = 0.001 Bohr, energy shift = 0.001 Ry, Delta rinn = 0.8, $v_0 = 40.0$ Ry and split norm = 0.15; (iii) Iteration control parameters: Tolerance = 10^{-5}, Criterion = total energy and max steps = 500; (iv) two probe algorithm parameters: Electrode constraint = off and initial density type = equivalent bulk; (v) Energy contour integral parameters: Circle points = 30, Integral lower bound = 3 Ry, Fermi line points = 10, Fermi function poles = 4, real axis infinitesimal = 0.01 eV and real axis point density = 0.02 eV; (vi) Two center integral parameters: Cutoff = 2500.0 Ry and points = 1024.

In the present study, we choose linear polyaromatic hydrocarbons Anthracene ($C_{14}H_{10}$) (Ref. Fig. 1), which is essentially a molecular organic semiconductor. It is a solid polycyclic aromatic hydrocarbon consisting of three fused benzene rings and can be used as a scintillator for detectors of high energy photons, electrons and alpha particles.

III. RESULTS AND DISCUSSION

A. System of armchair graphene ribbon

We calculated the system properties of bare AGNR and AGNR with attached bio-objects. The band structure energy (BSE), i.e., the sum of the energies of all states weighted with their respective occupation for bare AGNR is found as −1548.21 eV, whereas for AGNR with attached bio-objects, it is about −1946.59 eV. The calculated charge

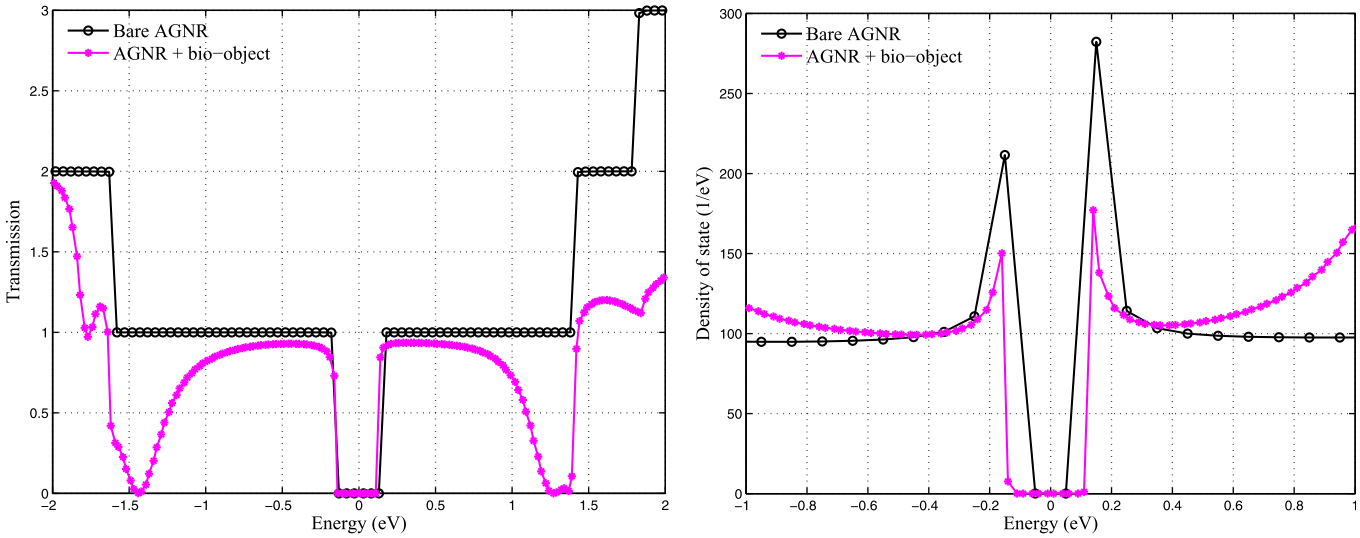

(a) Transmission for bare AGNR (5,5) of 9 unit cells and the same AGNR with attached organic-fragment

(b) Density of states

FIG. 2. Comparison of (a) transmission for bare (5, 5) AGNR with AGNR attached bio-object, as a function of energy at equilibrium. The calculation was performed at ambient temperature, $T = 300$ K. The band structure energy for bare AGNR is found as -1548.21 eV, whereas for AGNR with attached organic molecule, this increases to -1946.59 eV. At the energy range of about ± 0.2 eV, there is one conducting channel which results in a unit transmission coefficient; and (b) density of states for the bare (5, 5) AGNR and the same AGNR with attached polyaromatic hydrocarbons.

of bare AGNR is about $175.96q$ (where q is the electronic charge), compared to a charge of $219.94q$ in the case of AGNR with attached bio-objects. Fig. 2 compares the estimated transmission for the bare AGNR with bio-object attached in AGNR. Here, T represents the sum of the probabilities of transmission between the two electrodes for different eigenchannels. Since in the absence of tunneling, no transmission can occur in the energy window between the quasi-Fermi levels of the electrodes, the transmission coefficient in this window is essentially zero. The energy reference is at the Fermi energy. It is clear that the AGNR exhibits semiconducting behavior. The states contributing to the conduction have a range of energy of about ± 0.2 eV in this case. A similar characteristic for bare graphene has been reported in a recent study.[20] Now we explain the mechanism of transport phenomenon for an explanation for the features of the $(I - V)$ characteristics.

As the applied bias is increased and exceed the band-gap free states of the right electrode become available and then starts contributing to the electrode-electrode tunneling. This mechanism makes sudden increase in the current when $V \geq 0.3$. The effect of hydrocarbon attachment on the conductance of the AGNR considered here is summarized in Fig. 3. It is clear that in all the cases the current increases with bias. It is interesting to note that our results for the interaction between hydrocarbons and semiconducting ribbons demonstrate a clear increase in the conductance $(G = I/V)$ of semiconducting ribbons. The inset figures of Fig. 3 show significant increase in the $I - V$ curves of AGNR and AGNR with attached organic-molecules. For the semiconducting-AGNR system, there exists almost zero current plateau with a threshold voltage $V \approx 0.3$ as shown in Fig. 3. This phenomenon originates from the semiconducting states observed by state gap in Fig. 2(b), because an electron at the highest valance can jump to the Fermi energy and take part into the role of transport mechanism when its absorbed energy as $V \geq 0.3$. Similar phenomenon can be observed in Ref. 40. It is found that the transmission $T(E, V)$ contributing to the current always rests at near unity for applied bias $0 - 0.3$ V. However, we did not find any non-linearity in the I-V for the case considered in this study. Similar characteristics are also observed for other AGNR system.[41]

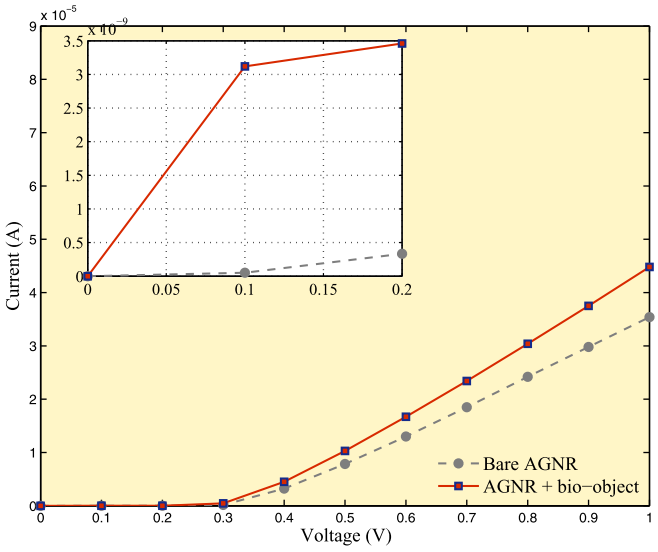

FIG. 3. I–V characteristics for the bare AGNR (5, 5) of nine unit cells in length and the same AGNR with attached polyaromatic hydrocarbons. The inset figures show increase in current.

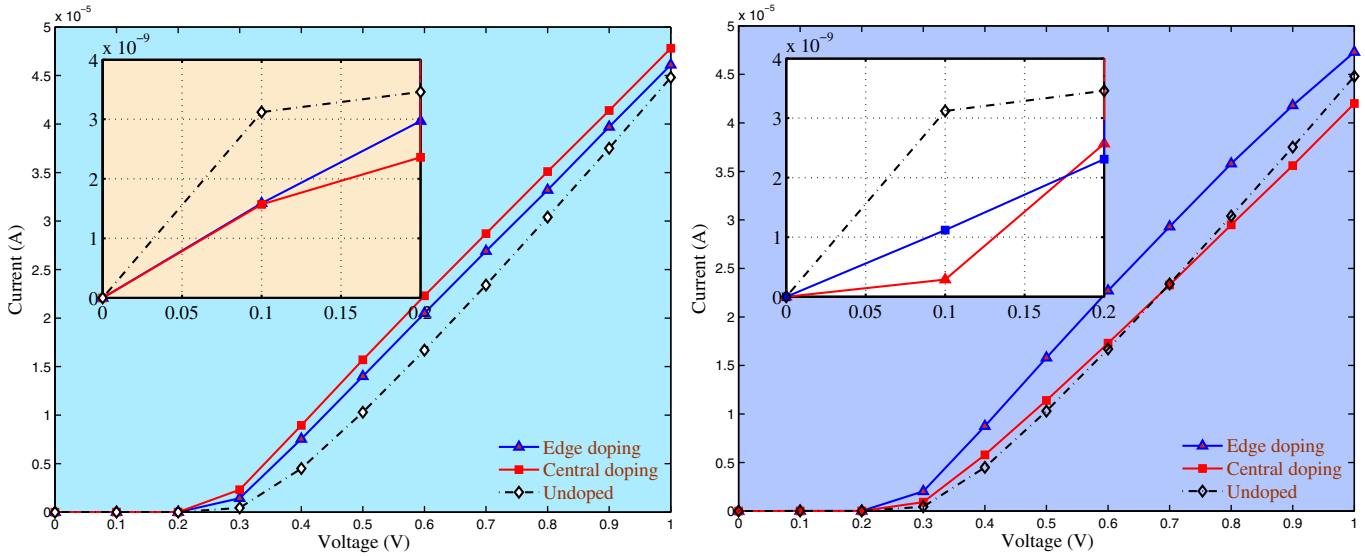

(a) Doping with Boron (b) Doping with Nitrogen

FIG. 4. I–V characteristics (a) for boron and (b) nitrogen doped at centre and edge of AGNR with attached polyaromatic hydrocarbon.

1. Effect of doping

In this section, we examined the effect of doping on AGNR with attached bio-object. The BSE for boron doped at the centre is found as −1824.91 eV, whereas for doped at the edge, it is about −1842.39 eV. Clearly there is no significant difference in band energies. However, compared to the un-doped system, the band energy of the doped system reduces to about 120 eV. Similarly, for nitrogen doping at the centre the BSE is found as −2059.28 eV, whereas for doping at the edge, it is about −2017.97 eV. This clearly demonstrates that, nitrogen doping increases the band energy about 110 eV. Fig. 4 shows the $I-V$ characteristics of the $(5,5)$ ribbon with an attached bio-objet, both boron and nitrogen doping. We observe the same trend of the current with increasing bias as mentioned above. We notice that the effect of the edge doping has a strictly increasing pattern, whereas for central doping current is virtually bias independent from $V = 0.0$ to $V = 0.2$ and the numerical value of the current is almost tends to zero. When V exceeds 0.2, the current starts to increase with the applied bias. The effect of doping on the density of states is summarized in Fig. 5. It can be observed that the doping of nitrogen at ribbon edge is significantly higher than others. This may be attributed that edge nitrogen is able to inject more states into the system. The calculated charge of central and edge doping due to boron is about $218.87q$ and $218.86q$, respectively, whereas, due to nitrogen doping it is about $220.98q$ and $220.99q$, respectively. Fig. 6 compares the estimated transmission coefficient for the bare AGNR with bio-object attached in AGNR with doping. It can be observed that edge-doping with nitrogen provides higher current than its central-doping counterpart. Similarly, central-doping with boron provides higher current

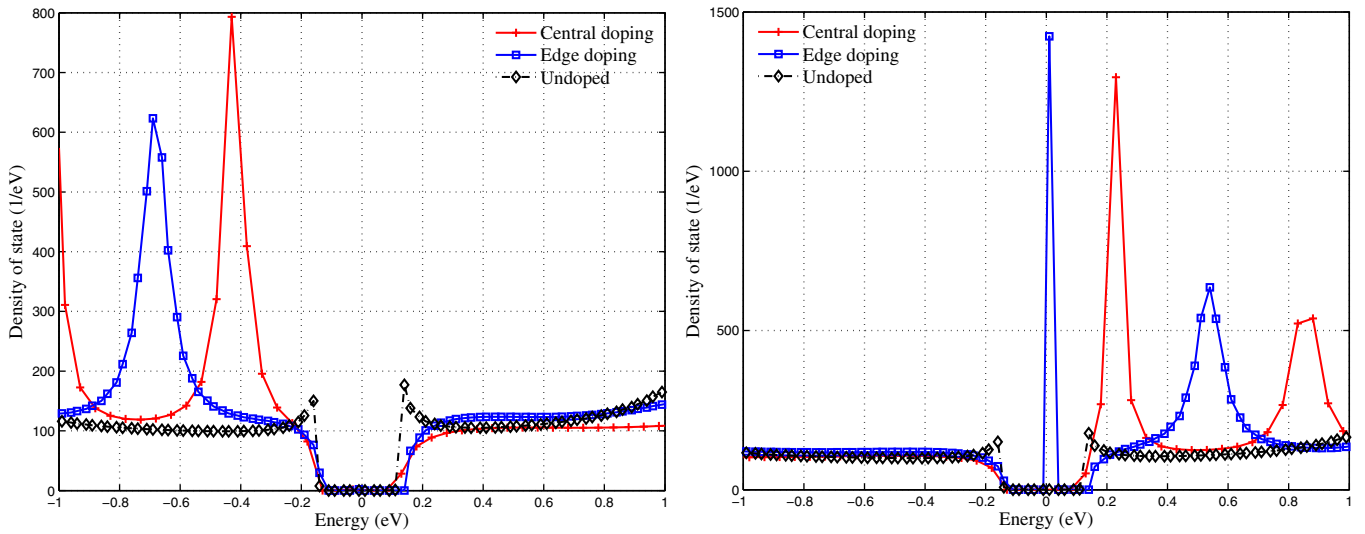

(a) Doping with Boron (b) Doping with Nitrogen

FIG. 5. Density of states (a) for boron and (b) nitrogen doped at centre and edge of AGNR with attached polyaromatic hydrocarbon.

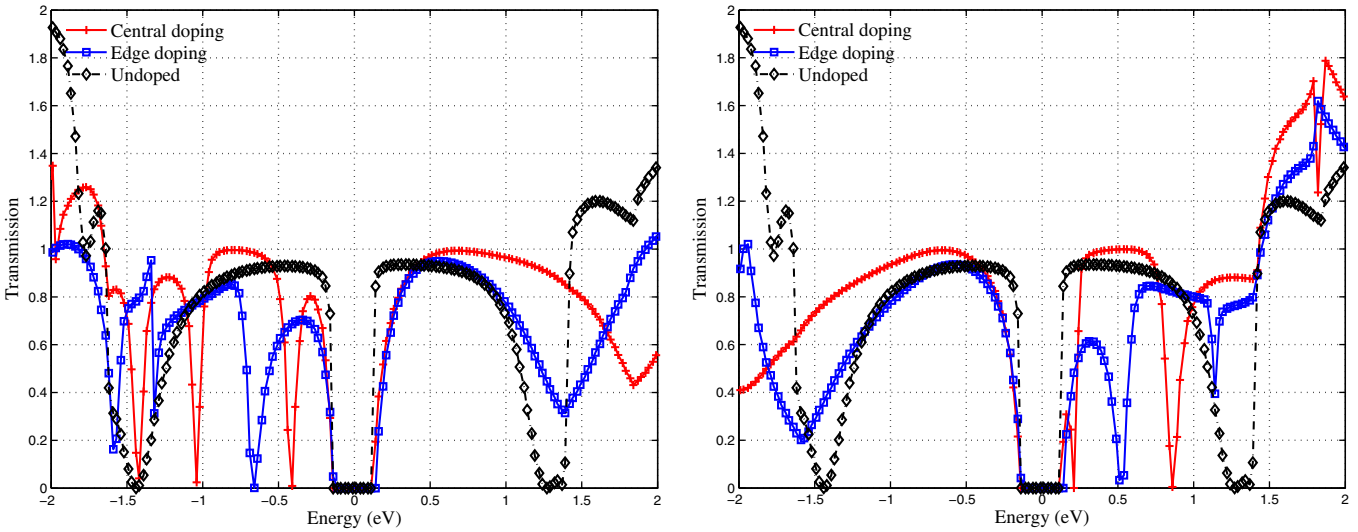

(a) Doping with Boron (b) Doping with Nitrogen

FIG. 6. Comparison of transmission (a) for boron and (b) nitrogen doped at centre and edge of AGNR with attached polyaromatic hydrocarbon.

than its edge-doping counterpart. For nitrogen doping, the calculated substitution energy at edge is less than that of central position. This clearly indicates that an energetic preference of nitrogen is at the edge position. Therefore, the required energy to overcome a Coulomb blockade for the system with nitrogen at edge-doping provides more current. Furthermore, this may be attributed to the fact that edge nitrogen is able to inject more states into the system. Similar argument can be made for boron-doped system. For the case of boron doping, the corresponding substitution energy at central position is less than that of edge position. Therefore, it can be argued that central doping with boron provides most energetically favorable configuration.

We observe that for $V = 0 - 0.1$ current is always linearly increasing in all cases. We notice that the effect of the edge doping has a strictly increasing pattern, whereas the central doping current has similar trend for from $V = 0$ to $V = 0.1$ for nitrogen doped system. For boron doped system, central doping current is virtually bias independent from $V = 0$ to $V = 0.1$. It can also be observed that, for nitrogen doped system, current transmission due to edge doping is much greater compared to the undoped system at $V \geq 0.3$. In contrast, central doping makes a reduction in current transmission. For small applied voltage, however, the transmission of current in the doped system is always lower than the undoped system. This may be attributed to the fact that edge nitrogen is able to inject more states into the system (see Fig. 5(b)).

The calculations of DOS have suggested that boron doped grapheme has weak interaction at near Fermi level between the molecules and the graphene. Such weak interactions are evident in their DOS structures (Fig. 5(a)), which show little change. The contribution of the Anthracene electronic levels on boron doped system is localized between -0.6 and -0.25 eV in the valence bands for central doping, which is just above the Fermi level. Due to this, it is expected to increase the conductance and evidenced by Fig. 4(a). With edge doping, DOS for the systems is localized between -0.8 and -0.45 eV in the valence bands, which is away from the Fermi level. Similarly, for nitrogen doped system localization occurs around Fermi level and between 0.4 and 0.7 eV (conduction band) with edge doping. This peak indicates that the system is strongly metallic and a significant increase in conductivity compared to the undoped system is expected. The change in the DOS, especially the area near the Fermi level, is expected to bring about obvious changes in the corresponding electronic properties. Therefore, it is concluded from Fig. 5 that boron doping at central position and nitrogen doping at edge are suitable for sensing applications of bio-molecules.

Present results suggest that the doped graphene exhibit much improved sensing properties than the undoped grapheme. It is worth noting that the strong binding between the chemical modification of graphene and certain molecules may also bring about some drawbacks. For example, strong binding implies that the removal of chemisorption of the biomolecules from the doped graphene could be difficult and the devices may suffer from longer recovery times. Finally, it can be pointed out that graphene-based sensor device is still in its early stages and much work is needed before it may compete with the many currently available sensors. A fundamental understanding of the binding phenomena of different bio-molecules on graphene is essential to explore this new field.

IV. CONCLUSION

In this work, we demonstrated that AGNRs show a clear change in conductance in response to the attachment of aromatic molecule. We also studied the effect of doping on the energy states as well transport properties of GNR with attached bio-objects. There exist different transport mechanisms depending on the applied bias. This type of structures seems to be useful to describe, qualitatively, the effects on the transport properties of AGNR when aromatic molecules attached to the ribbon edges. The energy states and

transmission of the AGNR suggests that AGNR can be used as a spectrograph sensor device. Additionally, significant effect of doping on these quasi-one dimensional system can be observed in the transmission spectrum. Based on these results, one may propose an extended and more detailed study of these nanostructures acting as nano-sensor devices. An interesting task would be to investigate the effect of large number of molecules randomly distributed along the ribbon edges on transport properties of these hybrid systems. A systematic analysis following this line may be useful to determine the type and concentration of foreign entities which could be detected with these kinds of structures.

[1]Y. Gan, W. Chu, and L. Qiao, "Stm investigation on interaction between superstructure and grain boundary in graphite," Surf. Sci. **539**, 120–128 (2003).
[2]A. K. Geim and K. S. Novoselov, "The rise of graphene," Nature Mater. **6**, 183–191 (2007).
[3]I. W. Frank, D. M. Tanenbaum, A. M. Van der Zande, and P. L. McEuen, "Mechanical properties of suspended graphene sheets," J. Vac. Sci. Technol. B **25**, 2558–2561 (2007).
[4]C. Lee, X. Wei, J. W. Kysar, and J. Hone, "Measurement of the elastic properties and intrinsic strength of monolayer graphene," Science **321**, 385–388 (2008).
[5]C. Chen, S. Rosenblatt, K. I. Bolotin, W. Kalb, P. Kim, I. Kymissis, H. L. Stormer, T. F. Heinz, and J. Hone, "Performance of monolayer graphene nanomechanical resonators with electrical readout," Nat. Nanomater. **4**, 861–867 (2009).
[6]F. Scarpa, S. Adhikari, and A. S. Phani, "Effective elastic mechanical properties of single layer graphene sheets," Nanotechnology **20**, 065709 (2009).
[7]C. L. Wong, M. Annamalai, Z. Q. Wang, and M. Palaniapan, "Characterization of nanomechanical graphene drum structures," J. Micromech. Microeng. **20**, 115029 (2010).
[8]F. Scarpa, S. Adhikari, and R. Chowdhury, "The transverse elasticity of bilayer graphene," Phys. Lett. A **374**, 2053–2057 (2010).
[9]X. Liu, T. H. Metcalf, J. T. Robinson, B. H. Houston, and F. Scarpa, "Shear modulus of monolayer graphene prepared by chemical vapor deposition," Nano Lett. **12**(2), 1013–1017 (2012).
[10]B. Biel, X. Blase, F. Triozon, and S. Roche, "Anomalous doping effects on charge transport in graphene nanoribbons," Phys. Rev. Lett. **102**, 096803 (2009).
[11]V. V. Cheianov and V. I. Fal'ko, "Selective transmission of dirac electrons and ballistic magnetoresistance of *n-p* junctions in graphene," Phys. Rev. B **74**, 041403 (2006).
[12]E. Prodan and R. Car, "Theory of tunneling transport in periodic chains," Phys. Rev. B **80**, 035124 (2009).
[13]N. Stander, B. Huard, and D. Goldhaber-Gordon, "Evidence for klein tunneling in graphene *p-n* junctions," Phys. Rev. Lett. **102**, 026807 (2009).
[14]A. H. Castro Neto, F. Guinea, N. M. R. Peres, K. S. Novoselov, and A. K. Geim, "The electronic properties of graphene," Rev. Mod. Phys. **81**, 109–162 (2009).
[15]J. Park, H. Yang, K. S. Park, and E.-K. Lee, "Effects of nonmagnetic impurities on the spin transport property of a graphene nanoribbon device," J. Chem. Phys. **130**, 214103 (2009).
[16]H. B. Heersche, P. Jarillo-Herrero, J. B. Oostinga, L. M. K. Vandersypen, and A. F. Morpurgo, "Bipolar supercurrent in graphene," Nature **446**, 56–59 (2007).
[17]S. K. Maiti, "Electron transport through honeycomb lattice ribbons with armchair edges," Solid State Commun. **149**, 973–977 (2009).
[18]R. Chowdhury and S. Adhikari, "Boron nitride nanotubes as zeptogram-scale bio-nano sensors: Theoretical investigations," IEEE Trans. Nanotechnol. **10**, 659–667 (2011).
[19]S. Adhikari and R. Chowdhury, "The calibration of carbon nanotube based bio-nano sensors," J. Appl. Phys. **107**, 124322 (2010).
[20]R. Chowdhury, S. Adhikari, P. Rees, S. P. Wilks, and F. Scarpa, "Graphene-based biosensor using transport properties," Phys. Rev. B **83**, 045401 (2011).
[21]Z. Zhang, B. Liu, K.-C. Hwang, and H. Gao, "Surface-adsorption-induced bending behaviors of graphene nanoribbons," Appl. Phys. Lett. **98**, 121909 (2011).
[22]M. Z. S. Flores, P. A. S. Autreto, S. B. Legoas, and D. S. Galvao, "Graphene to graphane: A theoretical study," Nanotechnology **20**, 465704 (2009).
[23]D. V. Kosynkin, A. L. Higginbotham, A. Sinitskii, J. R. Lomeda, A. Dimiev, B. K. Price, and J. M. Tour, "Longitudinal unzipping of carbon nanotubes to form graphene nanoribbons," Nature **458**, 872 (2009).
[24]P. Kumar, L. S. Panchakarla, and C. N. R. Rao, "Laser-induced unzipping of carbon nanotubes to yield graphene nanoribbons," Nanoscale **3**, 2127–2129 (2011).
[25]J. Cai, P. Ruffieux, R. Jaafar, M. Bieri, T. Braun, S. Blankenburg, M. Muoth, A. P. Seitsonen, M. Saleh, X. Feng, K. Muellen, and R. Fasel, "Atomically precise bottom-up fabrication of graphene nanoribbons," Nature **466**, 470–473 (2010).
[26]L. Jiao, X. Wang, G. Diankov, H. Wang, and H. Dai, "Facile synthesis of high-quality graphene nanoribbons," Nat. Nanotechnol. **5**, 321–325 (2010).
[27]L. Doessel, L. Gherghel, X. Feng, and K. Muellen, "Graphene nanoribbons by chemists: Nanometer-sized, soluble, and defect-free," Angew. Chem., Int. Ed. **50**, 2540–2543 (2011).
[28]A. V. Talyzin, I. V. Anoshkin, A. V. Krasheninnikov, R. M. Nieminen, A. G. Nasibulin, H. Jiang, and E. I. Kauppinen, "Synthesis of graphene nanoribbons encapsulated in single-walled carbon nanotubes," Nano Lett. **11**, 4352–4356 (2011).
[29]K. Wakabayashi, K.-I. Sasaki, T. Nakanishi, and T. Enoki, "Electronic states of graphene nanoribbons and analytical solutions," Sci. Technol. Adv. Mater. **11**, 054504 (2010).
[30]Atomistix ToolKit version 11.8, Quantumwise A/S (www.quantumwise.com).
[31]J. Perdew and A. Zunger, "Self-interaction correction to density-functional approximations for many-electron systems," Phys. Rev. B **23**, 5048–5079 (1981).
[32]N. Troullier and J. L. Martins, "Efficient pseudopotentials for plane-wave calculations," Phys. Rev. B **43**, 1993–2006 (1991).
[33]J. Soler, E. Artacho, J. Gale, A. Garcia, J. Junquera, P. Ordejon, and D. Sanchez-Portal, "The siesta method for ab initio order-n materials simulation," J. Phys.: Condens. Matter **14**, 2745–2779 (2002).
[34]G. B. Abadir, K. Walus, and D. L. Pulfrey, "Comment on 'curvature effects on electronic properties of small radius nanotube' [Appl. Phys. Lett. **91**, 033102 (2007)]," Appl. Phys. Lett. **94**, 176101 (2009).
[35]D. Michalska, L. J. Schaad, P. Carsky, B. A. Hess, and C. S. Ewig, "Basis set effects and the choice of reference geometry in abinitio calculations of vibrational-spectra," J. Comput. Chem. **9**, 495–504 (1988).
[36]R. Chowdhury, "Conductance of graphene nanoribbons under mechanical deformation," Physica E **44**, 1256 (2012).
[37]G. B. Abadir, K. Walus, and D. L. Pulfrey, "Bias-dependent amino-acid-induced conductance changes in short semi-metallic carbon nanotubes," Nanotechnology **21**, 015202 (2010).
[38]J. Taylor, H. Guo, and J. Wang, "Ab initio modeling of quantum transport properties of molecular electronic devices," Phys. Rev. B **63**, 245407 (2001).
[39]Y. Meir and N. S. Wingreen, "Landauer formula for the current through an interacting electron region," Phys. Rev. Lett. **68**, 2512–2515 (1992).
[40]X. Chen, H. Wang, H. Wan, K. Song, and G. Zhou, "Semiconducting states and transport in metallic armchair-edged graphene nanoribbons," J. Phys.: Condens. Matter **23**, 315304 (2011).
[41]M. Topsakal, V. M. K. Bagci, and S. Ciraci, "Current-voltage (*i-v*) characteristics of armchair graphene nanoribbons under uniaxial strain," Phys. Rev. B **81**, 205437 (2010).